Formation of doubly excited two-electron ions during $F^{8+}+He$, $F^{8+}+Ne$, and $F^{8+}+Ar$ collisions

Philip L. Pepmiller,* Patrick Richard, J. Newcomb,† James Hall, and T. R. Dillingham
James R. Macdonald Laboratory, Department of Physics, Kansas State University, Manhattan, Kansas 66506
(Received 28 November 1983)

High-resolution x-ray spectroscopy has been used to measure the cross sections for forming doubly excited F^{7+} ions in the $2s\,2p$ and $2p^2$ configurations following $F^{8+}+He$, $F^{8+}+Ne$, and $F^{8+}+Ar$ collisions over a projectile-energy range of 13—31 MeV. The intermediate states are found to be formed predominantly by projectile-electron excitation coupled with target-to-projectile electron transfer to an excited state during a single ion-atom collision. This process is termed nonresonant transfer and excitation (NTE) [P. L. Pepmiller *et al.*, IEEE Trans. Nucl. Sci. **NS-30**, 1002 (1983)]. A competing process for formation of the doubly excited states is resonant transfer and excitation (RTE) [D. Brandt, Phys. Rev. A **27**, 1314 (1983)], a process analogous to dielectronic recombination. Although the projectile energies spanned the region where resonant transfer and excitation are expected to maximize, no resonant contribution to the measured cross sections could be positively identified for the collision systems studied here. This result is consistent with the relative magnitudes of the theoretical cross sections for resonant and nonresonant transfer and excitation presented in the present work.

I. INTRODUCTION

The formation of inner-shell doubly excited states in atoms or ions has been investigated primarily as a sidelight to other studies of such topics as atmospheric physics,[1,2] astrophysical spectra,[3] fusion plasma research,[4,5] and ion-atom collisions.[6,7] Such doubly excited states have been investigated by experimental techniques,[8] and theoretical models have been used to calculate the associated energy levels.[9–12] The question of what physical processes are responsible for producing these doubly excited states cannot be answered without a detailed comparison of experimental measurements and theoretical calculations. Two mechanisms for the formation of inner-shell doubly excited states associated with single-electron-capture events in ion-atom collisions are considered in the present work. One of these is a resonant process, analogous to dielectronic recombination, in which the capture of a quasifree electron provides the energy necessary to excite a bound electron. The other is a nonresonant process combining electron excitation and charge transfer in a single ion-atom collision.

The resonant process analogous to dielectronic recombination (DR) which may occur in ion-atom collisions was first proposed by Tanis *et al.*[13] This process differs from DR in that the input energy is provided by a moving ion while an electron bound to the target atom plays the role of the free electron. These changes necessitate some modifications in the theory, which will be discussed later, and means that the term dielectronic recombination is no longer strictly applicable. The term resonant transfer and excitation (RTE) has been suggested.[14] Two experiments by Tanis *et al.*[13,15] investigating RTE have been reported. Both experiments involved three-electron ions incident upon gas targets in which the RTE process was identified by observing a maximum in the coincidence between projectile K x rays and four-electron projectile ions as a function of beam energy.

The nonresonant hypothesis for the formation of doubly excited states is associated with conventional Coulomb electron excitation of the projectile coincident with electron transfer from the target to the projectile during a single collision. The interaction of the target nucleus with a projectile electron excites that electron to some higher state while the interaction between the projectile nucleus and a target electron captures that electron into some excited state of the projectile. It is this process, leading to doubly excited states, that will be termed nonresonant transfer and excitation (NTE).[16,17]

To investigate the relative importance of RTE and NTE in medium energy ion-atom collisions, a systematic study has been carried out for one electron fluorine ions (F^{8+}) incident on gas targets of He, Ne, and Ar. High resolution x-ray spectroscopy of the F x rays has been used to measure the cross sections for forming doubly excited intermediate states consisting of two L-shell electrons. The intermediate states consist of the $2s\,2p(^3P)$, $2s\,2p(^1P)$, $2p^2(^1S)$, $2p^2(^1D)$, and $2p^2(^3P)$ states. The K-x-ray transitions from these states are not separately resolved in the present experiment, but as a group are resolved from the nearby $2p$-$1s$ transition. These states can be formed by RTE [except for the $2p^2(^3P)$ state which is forbidden by spin and parity considerations when configuration mixing is neglected] or by the NTE combination of L-shell electron capture and K-shell-to-L-shell electron excitation. The predicted maximum in the RTE cross section is near a projectile energy of 20 MeV, so the experiment was performed in this region. The prelimi-

nary results of this experiment were reported at the Seventh Conference on the Application of Accelerators in Research and Industry, Denton, Texas, November 1982.[17]

II. EXPERIMENTAL PROCEDURE

A. Apparatus

The experimental work for this study was performed using the facilities of the James R. Macdonald Laboratory at Kansas State University. The apparatus and experimental procedure have been described in detail elsewhere,[18] so they will only be summarized here. Negative fluorine ions were extracted from a diode ion source and injected into a model EN tandem Van de Graaff accelerator. The accelerated beam was momentum analyzed by passing through a primary analyzing magnet yielding final beam energies in the 13-to-31-MeV range with final charge states of F^{3+} through F^{5+}. The desired F^{8+} charge state was then produced by passing the beam through a thin (~ 5 $\mu g/cm^2$) carbon post-stripping foil followed by a secondary analyzing magnet used to direct the beam to the experimental apparatus. Collimation of the beam was accomplished using an adjustable four-jaw aperture located one meter upstream of the interaction region followed by a 2-mm fixed diameter aperture located 14 cm before the target. The four-jaw aperture was used to define the beam size while the second aperture was used to block out beam scattered by the first set of slits. The interaction region consisted of a differentially pumped gas cell bracketed by a 2-mm-diam entrance aperture and a 3-mm-diameter exit aperture. These apertures acted as baffles to the target gas and allowed the background pressure in the beam line to be maintained at less that 10^{-6} Torr. The pressure within the gas cell was monitored by an MKS, Inc. Baratron capacitance manometer. After passing through the gas cell, the beam was collected in a Faraday cup located one meter beyond the interaction region.

The high-resolution spectra investigated in this study were obtained with an Applied Research Laboratory 4-in. curved crystal spectrometer.[19] The spectra with the highest resolution were taken with a mica crystal. The majority of the data collected was obtained with a rubidium acid phthalate (RAP) crystal which has sufficient resolution to separate the $2p$-$1s$ and $2p\,2l$-$1s\,2l$ transitions and has the advantage of having approximately 10 times the reflectivity of the mica crystal.[20] A thalium acid phthalate (TlAP) crystal was also considered, since it has even higher reflectivity. However, it proved unsuitable due to its low resolving power. X rays analyzed by the spectrometer were detected by a flow mode proportional counter operated at $+2100$ V using a P-10 (90% argon, 10% methane) gas mixture at atmospheric pressure contained behind a thin (2 μm) Mylar window.

Logic decisions concerning data collection were made in a Digital Equipment Corporation PDP-11/34 minicomputer interfaced to the apparatus by CAMAC (computer-aided measurement and control) electronics. The computer was used to monitor the integrated beam current, to read the scalars which accumulated x-ray counts and time spent per channel, and to position the spectrometer crystal-detector combination by means of a stepping motor.

B. Data acquisition

The experimental procedure consisted of (1) measuring the yield of x-ray counts versus target pressure in order to determine the range of linearity, (2) scanning an extended region of the x-ray spectrum in order to establish an x-ray energy calibration, and (3) taking repeated short spectrometer scans of the region of interest in order to obtain sufficient statistics.

The target pressure dependence was measured for each projectile-energy—target combination in order to ensure that the K x rays were created under single collision conditions. Target pressures were typically maintained at <150 mTorr. Residual gas in the vacuum system between the secondary analyzing magnet and the experimental apparatus was estimated to generate 0.1 to 0.2 % F^{7+} charge-state impurity for a 10-m beam path.

The extended region used to establish an x-ray energy calibration is shown in Fig. 1. This figure depicts a spectrometer scan of the x-ray energy range from 690 to 940 eV showing F K x rays emitted following a 20-MeV F^{8+} + Ne collision. The observed peaks are due to the singly excited heliumlike transitions $1s\,2p(^3P)$-$1s^2(^1S)$, $1s\,2p(^1P)$-$1s^2(^1S)$, $1s\,3p$-$1s^2$, $1s\,4p$-$1s^2$, and the hydrogenlike Lyman-α transition $2p$-$1s$. The energy range of the doubly excited heliumlike transitions is indicated, although it is impossible to distinguish a peak in this low statistics scan. An advantage of studying the x rays from these doubly excited intermediate states is their proximity to the Lyman-α x ray which provides a benchmark on which to base further measurements. The energy of the Lyman-α x ray is well known,[21] and the cross sections for producing the intermediate $2p$ state have been measured for a variety of collision systems.[22–24] It is evident from Fig. 1 that the cross sections for producing the doubly excited states are relatively small, thus requiring many repeated scans of the region of interest in order to obtain sufficient statistics to observe the peaks above background. Since the Lyman-α x ray is close in energy to the x rays emitted from the doubly excited states, these repeated scans need only cover a small region thereby greatly shortening the required data collection time. Figure 2 shows the sums of repeated short spectrometer scans of the x-ray energy range from 800 to 840 eV which includes the region of the F doubly excited states and the Lyman-α radiation. The data shown cover a projectile energy range from 15 to 31 MeV and graphically illustrate the increase in background as the incident energy is increased. In addition, the relative difference in the intensities of the hydrogenlike Lyman-α and the doubly excited heliumlike transitions is apparent. Figure 3 shows a comparison of the spectra following 21 MeV F^{8+} + He, Ne, and Ar collisions. A spectrum obtained using a mica crystal rather than an RAP crystal is also shown in Fig. 3.

The measured x-ray production cross sections and their

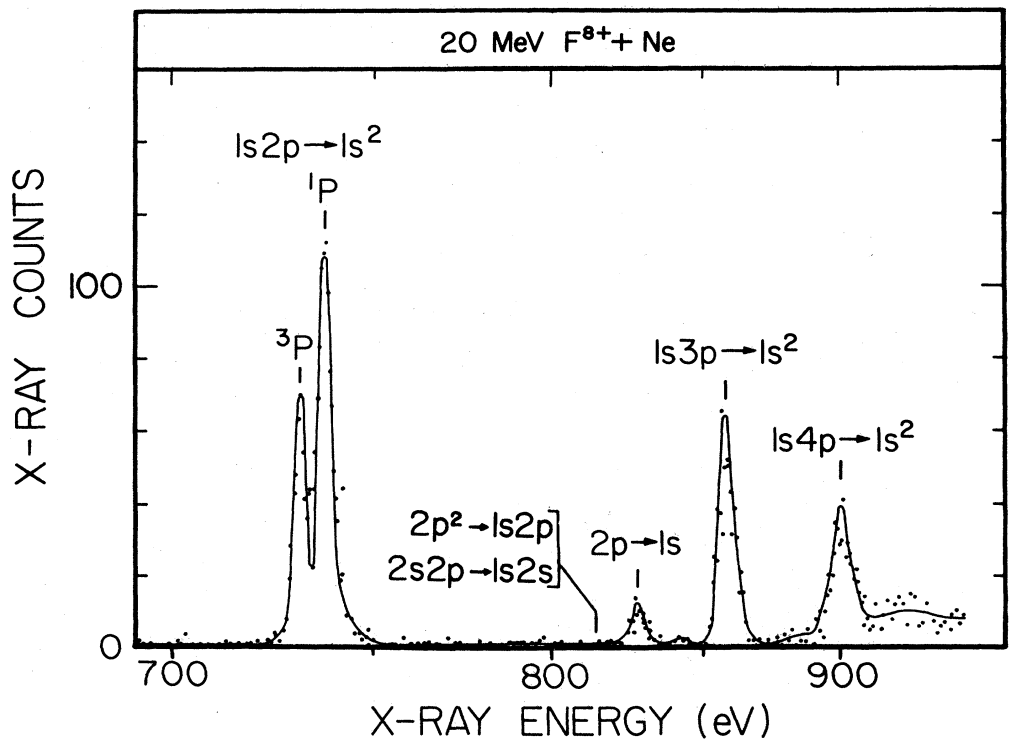

FIG. 1. High resolution scan of the x-ray energy range from 690 to 940 eV containing the F K x rays emitted following a 20 MeV F^{8+} + Ne collision is shown. The prominent peaks are due to electron capture to the $n=2$, 3, and 4 level. The small peak near 825 eV is due to $1s$-$2p$ electron excitation. The region of the x rays emitted from doubly excited $2p^2$ and $2s\,2p$ states is indicated.

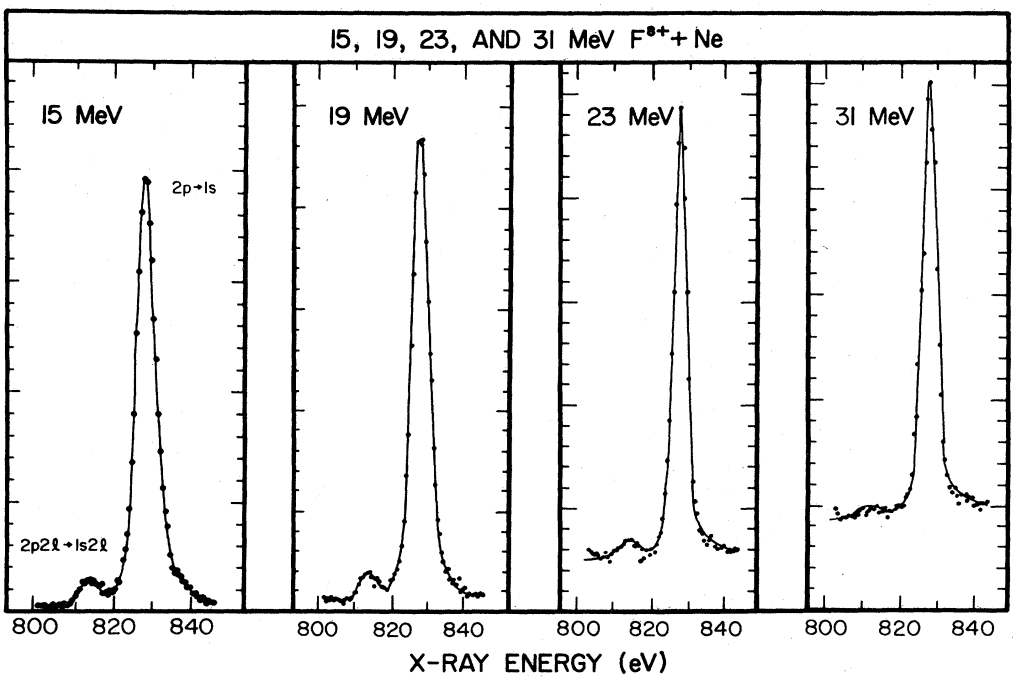

FIG. 2. Sums of repeated short spectrometer scans of the x-ray energy range covering the F doubly excited, two L-shell electron intermediate states, and the F Lyman-α are shown. The collision systems are 15, 19, 23, and 31 MeV F^{8+} + Ne. All of the spectra were obtained using a rubidium acid phthalate crystal. The absolute peak heights should not be compared from spectrum to spectrum since the gas pressure, current integrator scale, and number of spectrometer scans may vary.

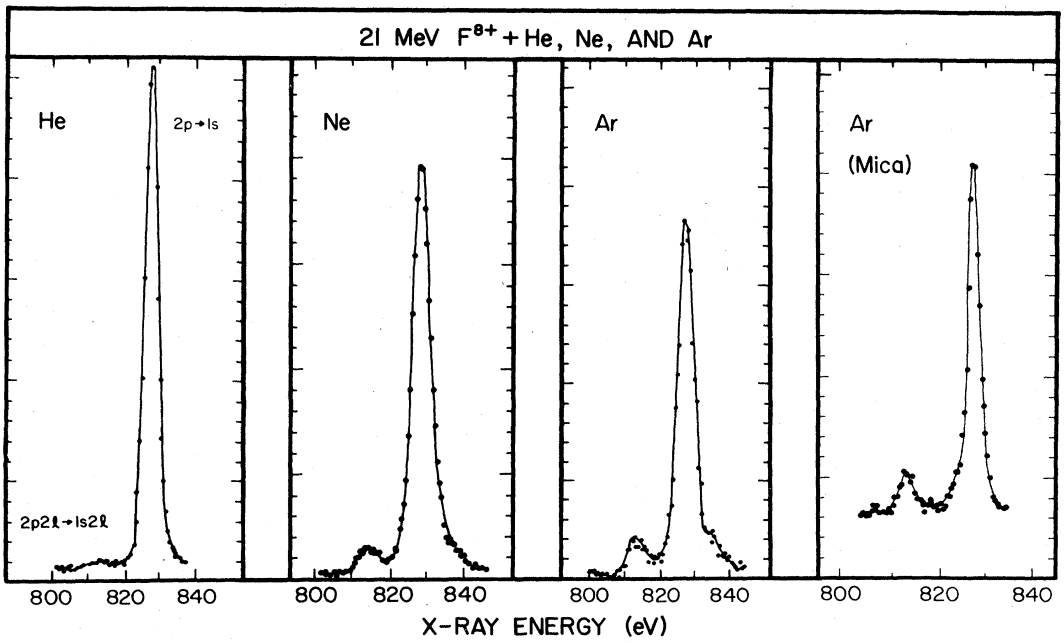

FIG. 3. Comparison of spectra from 21 MeV F^{8+} + He, Ne, and Ar collisions is shown. Three of the spectra were obtained using a rubidium acid phthalate crystal, and the fourth was obtained using a mica crystal. The improvement in the energy resolution and the increased background are apparent for the mica crystal.

associated errors are listed in Table I. The uncertainties in the measured cross sections stem from three major sources including counting statistics, background subtraction, and normalization to previous works. The errors from peak integration and background subtraction were added in quadrature. The normalization errors are dependent on the accuracy of the previous measurements.[22–24] The quoted uncertainly in the F^{8+} + He measurements of Tawara *et al.*[22] is on the order of 20%, while the uncertainty in the F^{8+} + Ne and Ar measurements of Richard *et al.*[23] and Brown *et al.*[24] are on the order of 50%.

III. THEORY

A. Resonant transfer excitation

The theoretical cross section for dielectronic recombination (DR) of an electron with an ion has been worked out in detail by several authors.[25–27] For a free electron interacting with a one electron ion, the DR theory predicts an on-resonance cross section of

$$\sigma_{\mathrm{DR}}(E_e)=\frac{\pi\hbar^3}{mE_A}\frac{(2L+1)(2S+1)\Gamma_A}{2(2l+1)(2s+1)}\omega\delta(E_A-E_e)\ , \tag{1}$$

where E_e is the energy of the electron relative to the ion, m is the mass of the electron, $L\,(S)$ is the orbital (spin) angular momentum of the initial state, $l\,(s)$ is the orbital (spin) angular momentum of the intermediate state, Γ_A is the Auger rate, ω is the fluorescence yield, and E_A is the resonance energy (i.e., the Auger-electron energy) of the intermediate state (l,s). As represented, $\sigma_{\mathrm{DR}}(E_e)$ is the cross section for capturing an electron into an excited state with the accompanying excitation of a bound electron, followed by radiative decay of the intermediate excited state. The cross section for forming the intermediate doubly excited state is given by $\sigma_{\mathrm{DR}}(E_e)/\omega$.

Resonant transfer and excitation (RTE) is distinguished from dielectronic recombination in that a bound or quasi-free electron rather than a free electron is involved.[13–17] In DR the usual picture is that of a free electron approaching a stationary ion. A change of coordinate system yields the alternative view of a moving ion incident

TABLE I. Measured total x-ray production cross sections in units of 10^{-20} cm^2 for doubly excited two-electron states ($2s\,2p$ or $2p^2$) formed during F^{8+} + He, F^{8+} + Ne, and F^{8+} + Ar collisions.

Energy (MeV)	He	Ne	Ar
13		0.6±0.10	
15	0.69±0.11	0.88±0.09	5.6±1.0
17	0.59±0.08	1.2±0.2	7.0±1.2
19	0.46±0.06	1.4±0.2	7.2±1.2
21	0.36±0.06	1.7±0.2	8.1±1.1
23		2.1±0.3	7.6±1.4
25	0.14±0.07		
27		2.5±0.4	
31		2.3±0.5	

on a stationary electron. The resonant energy for the process is now the energy that a moving ion is required to have in order to match the velocity an electron would have in DR with a stationary ion (i.e., the system must have the same relative velocity at resonance). For RTE, the bound electrons have, in addition, a distribution of velocities given by their Compton profile.[28] Experimentally this distribution proves beneficial since an incident ion with an off-resonance velocity can still participate in RTE if it encounters an electron which can make up the difference in velocity. However, this adds complications to the calculation of RTE cross sections in that a numerical integration over the electron's momenta must be performed. Furthermore, the distribution of electron velocities in the target rest frame gives rise to a broadening of the resonance curve.

The theory relating RTE cross sections to DR cross sections using the impulse approximation has been worked out in detail by Brandt.[14] The cross section for RTE followed by x-ray emission is given as a function of the incident ion energy E as

$$\sigma^{x}_{\mathrm{RTE}}(E)=(M/2E)^{1/2}\Delta\epsilon\,\bar{\sigma}_{\mathrm{DR}}\sum_{i}J_i(p_{iz})\,, \tag{2}$$

where M is the mass of the incident ion and $\bar{\sigma}_{DR}$ (which implicitly includes the fluorescence yield ω) is the DR cross section averaged over the energy interval $\Delta\epsilon$ containing the resonance energy E_A. The function $J_i(p_{iz})$ represents the Compton profile which gives the probability of finding a particular target electron with a momentum component

$$p_{iz}=(E_A-Em/M)(M/2E)^{1/2} \tag{3}$$

in the z (beam) direction. The summation in Eq. (2) extends over all target electrons.

The results of RTE calculations for x rays emitted from doubly excited states formed during a F^{8+} + He collision[29] are given in Fig. 4. As already discussed, this cross section shows a resonance behavior characteristic of a very sharply peaked DR cross section spread out by the Compton profile of the target electrons. The various curves are for the indicated intermediate two-electron states. RTE calculations summed over intermediate states produced in F^{8+} impact on three different targets (He, Ne, and Ar) are shown in Fig. 5. The broadening in the cross section for F^{8+} + Ne is due to the higher average binding energies of the Ne L-shell electrons as compared to the He K-shell electrons. The cross section for F^{8+} + Ar exhibits a more complex structure due to the sum of contributions from the Ar-target L and M shells. The Ar L shell is rather tightly bound so its Compton profile is much broader than that of the more loosely bound Ar M shell. the Ne and Ar K-shell electrons have been omitted from the calculation because their binding energies exceed the limits of the impulse approximation

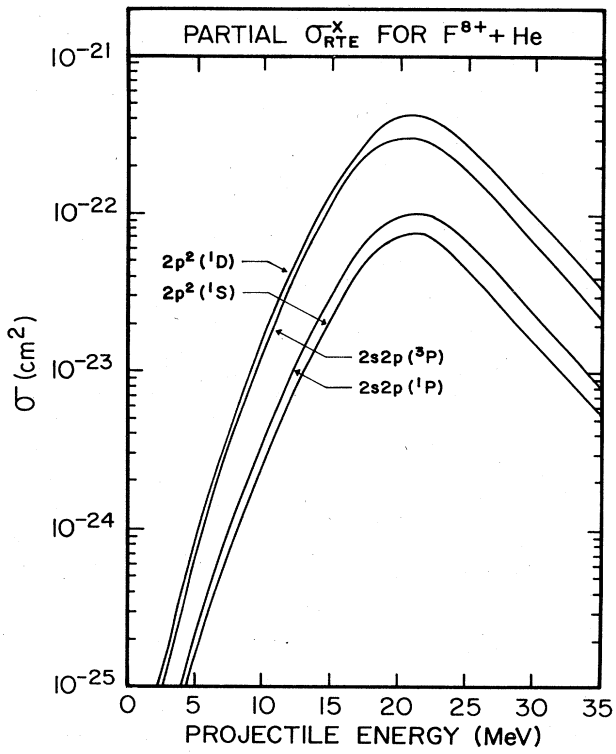

FIG. 4. Calculated partial RTE K-x-ray-production cross sections for F^{8+} + He are shown. This figure shows the predicted intensities of the four doubly excited states allowed by DR. The relative height of each resonance is determined by the DR cross section, while the width is determined by the Compton profile.

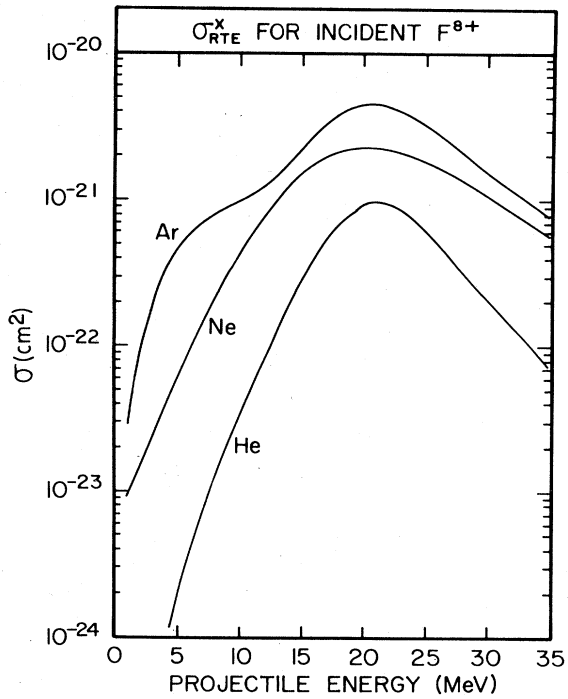

FIG. 5. Calculated RTE K x-ray production cross sections for F^{8+} + He, Ne, and Ar are shown. This figure gives K x-ray production cross sections summed over all doubly excited, two L-shell electron multiplets. The broadening in the resonances is due to the widths of the Compton profiles of the target electrons.

used in the derivation of the RTE cross sections.[14] Their inclusion would not significantly change the results reported here due to the relatively small number of electrons and the extreme width of their Compton profiles.

Table II is a collection of data relevant to the calculation of RTE cross sections for doubly excited two-electron fluorine ions. It includes a listing of the intermediate and final states, their corresponding x-ray[8] and Auger[30] decay energies, the corresponding beam resonance energies, the fluorescence yields,[31] and the calculated DR cross sections.[32]

B. Nonresonant transfer and excitation

In this section an approximate evaluation of the nonresonant transfer and excitation (NTE) cross section is described. In the impact parameter treatment of atomic collisions, the cross section for a given process can be expressed as

$$\sigma = 2\pi \int_0^\infty P(b) b \, db \ , \tag{4}$$

where $P(b)$ is the probability of the process occurring for a given impact parameter b. In NTE, a target electron is captured into an excited state of the projectile accompanied by Coulomb excitation of a projectile electron. The probability of these two independent events happening in the same collision is given by the product of their probabilities. Thus,

$$\sigma_{\mathrm{NTE}} = 2\pi \int_0^\infty P_{\mathrm{cap}}(b) P_{\mathrm{ex}}(b) b \, db \ , \tag{5}$$

where $P_{\mathrm{cap}}(b)$ is the probability of capture and $P_{\mathrm{ex}}(b)$ is the probability of excitation. $P_{\mathrm{cap}}(b)$ and $P_{\mathrm{ex}}(b)$ have different impact parameter dependences.[33,34] $P_{\mathrm{cap}}(b)$ decreases slightly in magnitude from b equal zero to the radius of the shell captured into, but drops off rapidly for larger b. $P_{\mathrm{ex}}(b)$ is relatively constant from b equal zero to the radius of the shell originally occupied, but also drops off rapidly for larger b. In this experiment the excitation is occurring from the K shell while the capture is to the L shell. The radius of the K shell is approximately one-fourth that of the L shell, so only within the K shell is the product $P_{\mathrm{cap}}(b)P_{\mathrm{ex}}(b)$ of appreciable magnitude. Equation (5) can then be approximated by

$$\sigma_{\mathrm{NTE}} \simeq 2\pi P_{\mathrm{cap}}(0) \int_0^\infty P_{\mathrm{ex}}(b) b \, db \ . \tag{6}$$

Noting that the excitation cross section can be represented by

$$\sigma_{\mathrm{ex}} = 2\pi \int_0^\infty P_{\mathrm{ex}}(b) b \, db \ , \tag{7}$$

we obtain

$$\sigma_{\mathrm{NTE}} = P_{\mathrm{cap}}(0) \sigma_{\mathrm{ex}} \ . \tag{8}$$

Finally, the cross section for x-ray emission from a particular intermediate state (l,s) can be expressed as

$$\sigma^x_{\mathrm{NTE}}(l,s) = P_{\mathrm{cap}}(0) \sigma_{\mathrm{ex}} S(l,s) \omega(l,s) \ , \tag{9}$$

where $\omega(l,s)$ is the fluorescence yield[31] and

$$S(l,s) = \frac{(2l+1)(2s+1)}{\sum_{ls} (2l+1)(2s+1)} \tag{10}$$

gives the relative population of the state under the assumption that the intermediate states are statistically populated.

The cross section for $1s$-$2p$ excitation, used in the evaluation of $\sigma^x_{\mathrm{NTE}}(l,s)$ in Eq. (9), has been measured previously for F^{8+} + He, Ne, and Ar.[22–24] An impact-parameter-dependent Brinkman-Kramers calculation was used to obtain $P_{\mathrm{cap}}(b)$.[33] $P_{\mathrm{cap}}(0)$, in Eq. (9), was taken to

TABLE II. Doubly excited states of F^{7+}.

Intermediate state	x-ray final state	Channel energy[a] (eV)	Auger final state	Channel energy[b] (eV)	Corresponding beam resonance energy (MeV)	Fluorescence yield[c] ($\times 100$)	DR cross sections[d] (10^{-20} cm^2)
$2s\,2p\,(^3P)$	$1s\,2s\,(^3S)$	814.4	$1s\,(^2S)$	597.3	20.8	21.5	4.0
$2s\,2p\,(^1P)$	$1s\,2s\,(^1S)$	818.1	$1s\,(^2S)$	610.9	21.3	21.8	1.3
$2p^2(^1S)$	$1s\,2p\,(^1P)$	818.1	$1s\,(^2S)$	617.7	21.5	5.8	1.0
$2p^2(^3P)$	$1s\,2p\,(^3P)$	813.2				100.0	0
$2p^2(^1D)$	$1s\,2p\,(^1P)$	811.0	$1s\,(^2S)$	609.5	21.3	2.4	5.4
$2p\,3s\,(^3P)$	$1s\,3s\,(^3S)$	824.0					
$2p\,3p\,(^3P)$	$1s\,3s\,(^3P)$	824.0					
$2p\,4s\,(^3P)$	$1s\,4s\,(^4S)$	826.1					
$2p\,4p\,(^3D)$	$1s\,4p\,(^3P)$	826.1					
Rydberg limit $2p\,\infty L$	$1s\,\infty L$	827.6	$1s\,(^2S)$	827.6	28.9		

[a]See Ref. 8.
[b]See Ref. 30.
[c]See Ref. 31.
[d]See Refs. 26 and 32.

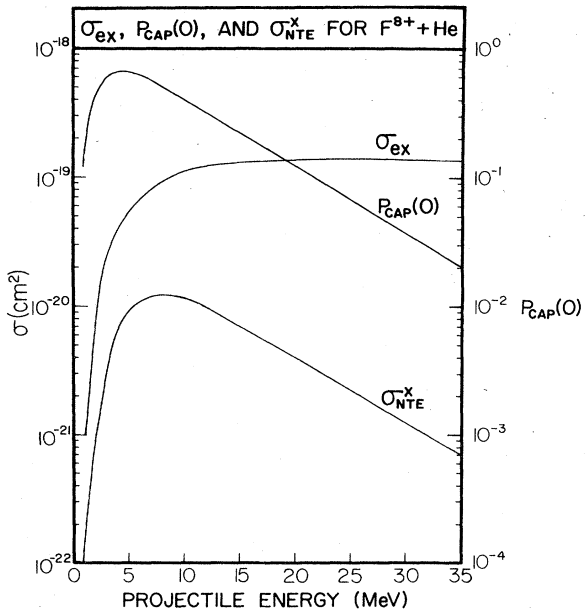

FIG. 6. Energy dependence of the electron excitation cross section, the NTE cross section, and the probability of capture for F^{8+} + He are shown. The scale on the right of the figure is for $P_{cap}(0)$, the average probability of capture at small impact parameters. The scale at the left of the figure is for the electron excitation cross sections, and for NTE, which is the product of the capture probability and the electron excitation cross section.

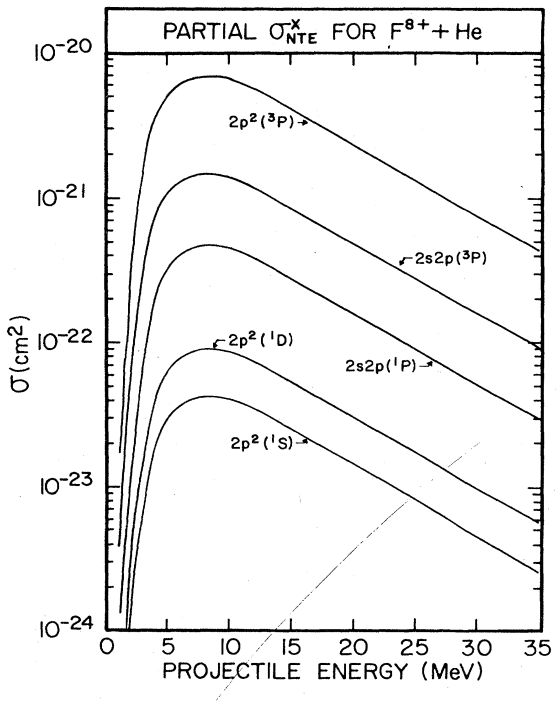

FIG. 7. Calculated partial NTE x-ray production cross sections for F^{8+} + He are shown. The predicted intensities given by the NTE theory are shown for the five multiplets formed by $2s2p$ and $2p^2$ intermediate states. The energy dependences of the multiplets are identical. The relative magnitudes of the cross sections are due to the statistical factors and the fluorescence yields.

be an average capture probability over the range from b equal to zero to b equal to 1.5 times the K-shell radius. The contributions of the electrons excitation cross section and the capture probability to the NTE cross section for the case of F^{8+} + He are shown in Fig. 6. The NTE cross section shown has been summed over all of the allowed intermediate states (l,s). It should be noted that the calculated value of $P_{cap}(0)$ has been renormalized by a factor of 0.74 for the case of F^{8+} + He for the purpose of comparison with experiment. This renormalization will be discussed in more detail in Sec. IV.

The result of the NTE calculation for the specific x rays emitted from the intermediate doubly excited states formed during a F^{8+} + He collision are shown in Fig. 7. The differences in the relative magnitudes of the cross sections are due to differences in the statistical factors and the multiplet term fluorescence yields for the various intermediate states.

The result of the NTE calculation for formation and decay of the sum of all allowed multiplets consisting of intermediate $2s2p$ or $2p^2$ states produced in F^{8+} + He, Ne, and Ar collisions is shown in Fig. 8. For the case of F^{8+} + He, the σ^x_{NTE} calculation has been extended to lower energies by extrapolating the measured excitation cross sections using a Born-approximation calculation.[35] However, for the cases of F^{8+} + Ne and Ar, it is known that the Born approximation fails to predict either the magnitude or the energy dependence of the excitation

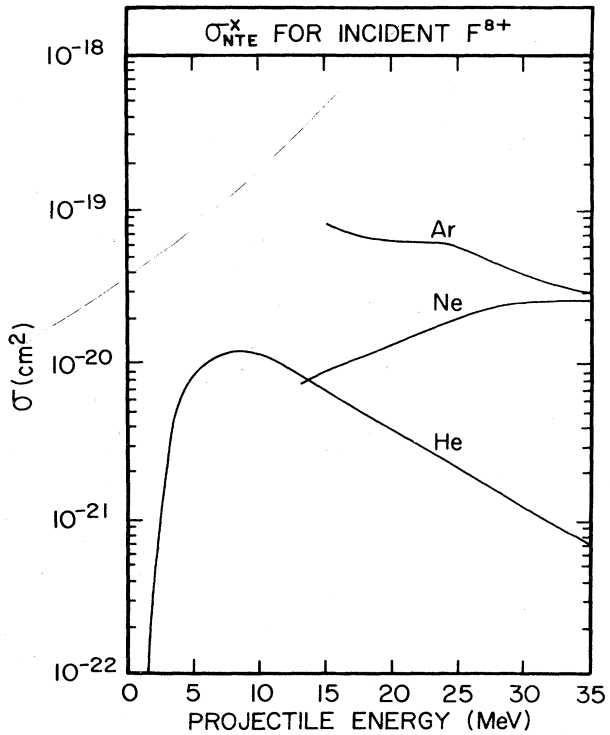

FIG. 8. Calculated NTE K x-ray production cross sections for F^{8+} + He, Ne, and Ar are shown. For the He target, the NTE cross sections calculated for the five multiplets graphed in the previous figure have been summed to obtain the total K x-ray production cross section for the $2s2p$ and $2p^2$ intermediate states. Similar calculations have been performed for the Ne and Ar targets.

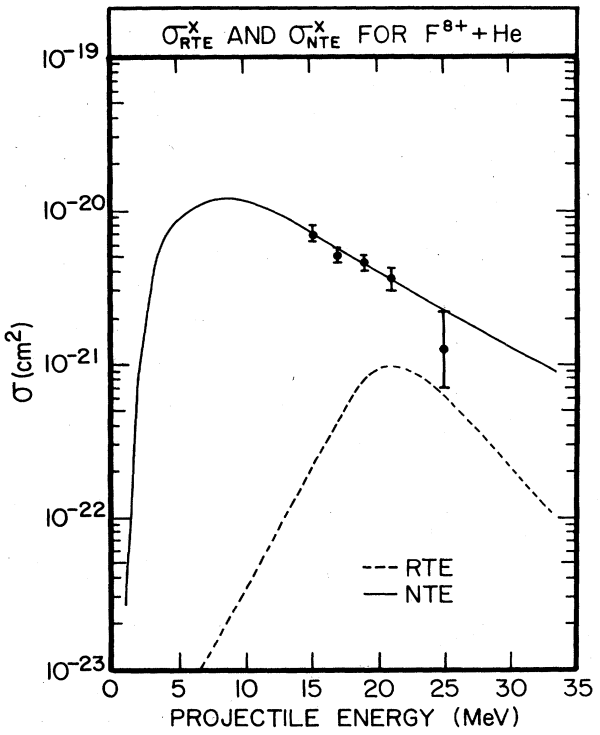

FIG. 9. Comparison of the experimental results with the RTE (dotted line) and NTE (solid line) theories for F^{8+} + He is shown.

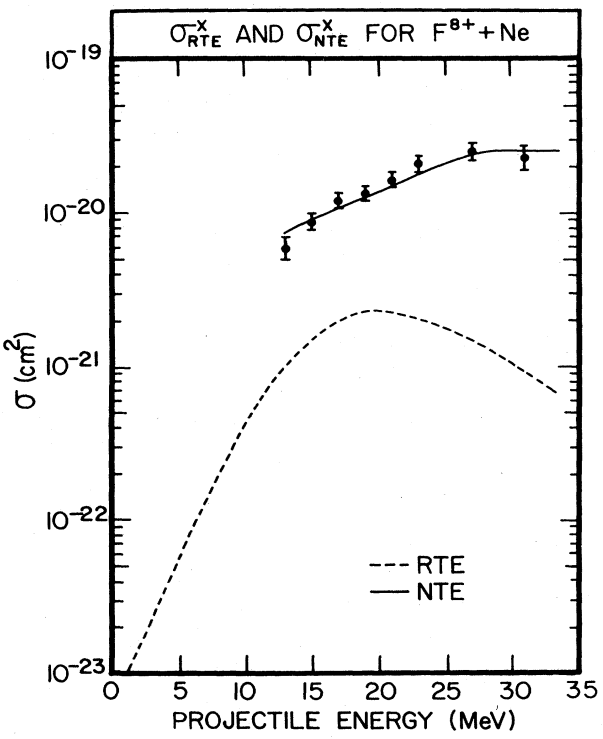

FIG. 10. Comparison of the experimental results with the RTE (dotted line) and NTE (solid line) theories for F^{8+} + Ne is shown. As was noted in the text, it is not possible to extend the NTE theory to lower projectile energies due to the absence of reliable calculated or measured electron excitation cross sections.

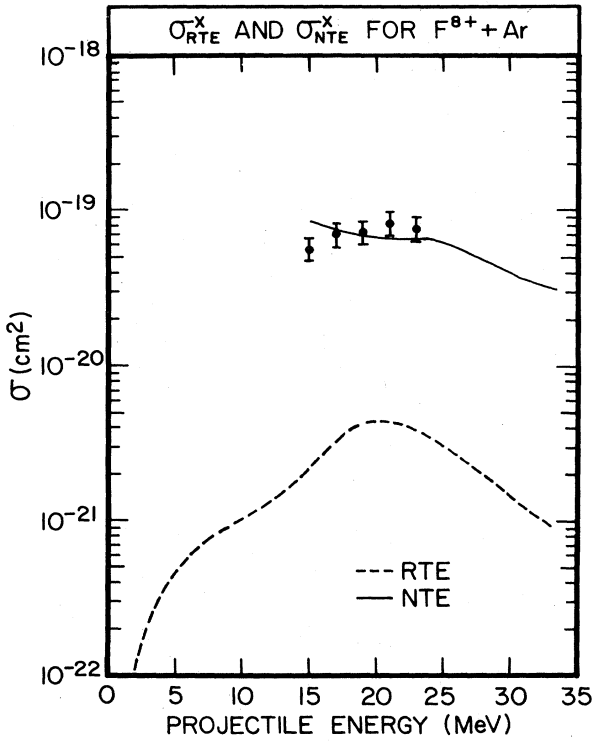

FIG. 11. Comparison of the experimental results with the RTE (dotted line) and NTE (solid line) theories for F^{8+} + Ar is shown. As was noted in the text, it is not possible to extend the NTE theory to lower projectile energies due to the absence of reliable calculated or measured electron excitation cross sections.

cross sections. Thus, due to the absence of reliable calculated or measured electron excitation cross sections, the NTE calculations cannot be extended to lower projectile energies for these cases. It should be noted that for the He and Ne targets the dominant contribution to $P_{cap}(0)$ in the NTE calculation is from the target K shell, while for the Ar target the dominant contribution is from the L shell.

IV. DISCUSSION

The previous two sections have presented the measured total x-ray production cross sections and have described the RTE and NTE theories. A comparison of the theoretical calculations with the data for F^{8+} + He, Ne, and Ar is shown in Figs. 9—11. The theoretical RTE cross sections are for the sum of the four doubly excited, two L-shell electron intermediate states allowed by dielectronic recombination. The theoretical NTE cross sections are for the sum of the five allowed doubly excited, two L-shell electron intermediate states. The calculated NTE cross sections have been scaled by $0.74[Z(\text{He})/Z(\text{target})]^2$ for the purpose of comparison with experiment. Scaling of the NTE cross sections is necessary because of the over-estimation of $P_{cap}(0)$ by the impact-parameter-dependent Oppenheimer-Brinkman-Kramers (OBK) cal-

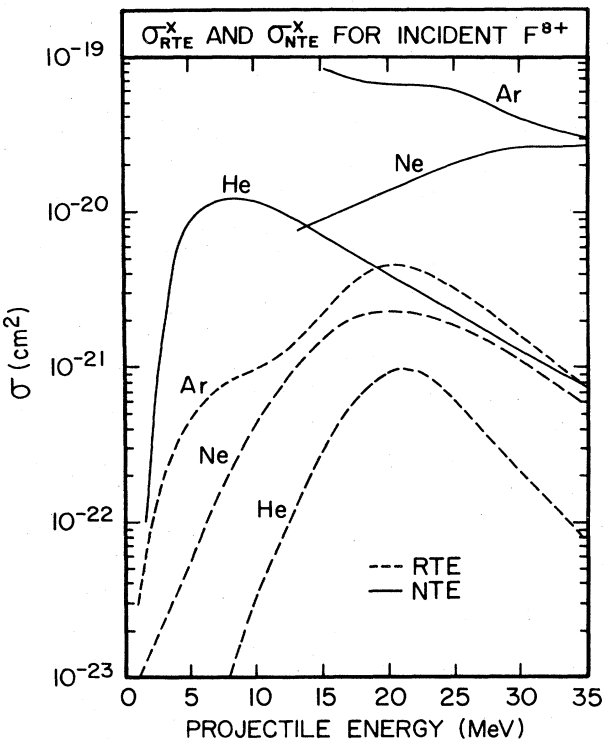

FIG. 12. Total K x-ray production cross sections for NTE (solid lines), and RTE (dotted lines) are compared for all three collision systems studied.

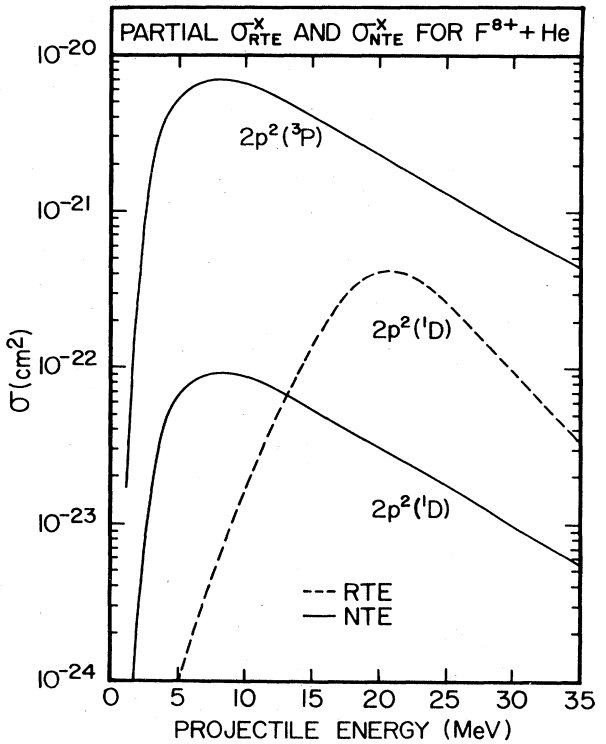

FIG. 13. Comparison of the relative contributions of RTE and NTE to the formation of the $2p^2(^1D)$ multiplet is shown. The NTE theory (solid line) predicts a low energy maximum followed by a steadily falling intensity. On resonance at a beam energy of 21 MeV the RTE theory (dotted line) predicts a larger cross section than the NTE theory. The $2p^2(^3P)$ multiplet is formed only by NTE (when configuration mixing is neglected) and has the largest cross section of all the five doubly excited states.

culation.[33] The scaling factors used in the present work are very near to the ratios of the measured total capture cross section to the OBK calculated total capture cross section for F^{8+} + He, Ne, and Ar.[36] It is apparent that the calculated RTE cross sections do not fit the energy dependence of the data, while the scaled NTE cross sections fit the data very well. Thus, although the projectile energies spanned the region where resonant transfer excitation is expected to maximize, no resonant contribution to the measured cross section can be positively identified in the present work. The RTE and NTE cross sections for the three targets are shown in Fig. 12 for the purpose of comparison.

It is proposed that by carefully minimizing background radiation and by obtaining higher resolution x-ray spectra in which the doubly excited states are energetically separated, it would be possible to separate the RTE and NTE contributions in F^{8+} + He. The separate curves for the multiplets are shown in Figs. 4 and 7. The predicted cross sections for the $2p^2(^3P)$ and $2p^2(^1D)$ states are shown in Fig. 13. The $2p^2(^3P)$ state is formed only by NTE. The RTE process does not contribute to the $2p^2(^3P)$ cross section (in the absence of configuration mixing) due to parity and spin conservation rules which apply to the inverse Auger process and presumably also to RTE. The $2p^2(^1D)$ state is formed by both NTE and RTE with RTE exceeding NTE near resonance. The energy dependence of the NTE process could then be deduced from the measured $2p^2(^1D)$ and $2p^2(^3P)$ cross sections. These measurements would also confirm the selection rules for RTE.

V. SUMMARY

This study of ion-atom collisions has utilized high resolution x-ray spectroscopy to study the formation and decay of doubly excited, two L-shell electron intermediate states formed during collisions involving one electron F^{8+} ions incident on neutral target atoms. The experimental range of beam energies centered on the region of the expected resonance in the calculated resonant transfer excitation cross section. However, in this series of experiments no evidence of this process could be positively identified. Again, this result is consistent with the relative magnitudes of the theoretical cross sections for resonant and nonresonant transfer excitation presented here. The process termed nonresonant transfer excitation appears to dominate in the formation of doubly excited, two L-shell electron intermediate states for the cases of F^{8+} + He, Ne, and Ar. The NTE cross section is due largely to the $2p^2(^3P)$ multiplet which has the combination of a large statistical factor and unit fluorescence yield. It is also apparent from the present study, as well as our preliminary results,[17] that RTE should be more prominent with lower Z targets (for example He). Recent studies by Clark *et al.*[37] using x-ray charge state coincidence techniques

with three-electron incident ions have shown that a large RTE contribution can be observed for heavier projectile ions ($Z=14$). The RTE peak for higher Z ions occurs at higher bombarding energies where the NTE cross section is greatly reduced due to the $\sim V^{-11}$ velocity dependence of the capture process.

We suggest two possible improvements that could be made on the present study that might provide more information about the relative importance of RTE and NTE. The first improvement, in view of the recent results of Clark *et al.*,[37] is to study the process with a one-electron Si beam. The corresponding RTE resonances occur at a higher bombarding energy where the relative importance of NTE is diminished. The energy required for this experiment unfortunately exceeds that which is available with the Kansas State University tandem. A second improvement is a higher resolution x-ray measurement as proposed in the previous section. An experiment which resolves the multiplet states would lay open for investigation the important selection rules for RTE and NTE and the effects of configuration mixing on RTE. The RTE contribution to the formation of the $2p^2(^1D)$ state is predicted to be larger than the NTE contribution on resonance. This, coupled with at most a small RTE contribution to the $2p^2(^3P)$ state, would make it possible to observe a resonance enhancement in the ratio of the ^1D to ^3P cross section. Currently available spectrometers utilizing position sensitive x-ray detectors provide the increased efficiency and energy resolution (~ 1 eV) necessary to make these measurements possible.

ACKNOWLEDGMENTS

The authors would like to thank Professor Tom J. Gray and Dr. Martin Stockli for helpful discussions and Kelly Jones for help provided in data collection. This work was supported by the U.S. Department of Energy, Division of Chemical Sciences.

*Present address: Physics Division, Oak Ridge National Laboratory, Oak Ridge, TN 37831.

†Present address: National Space Technology Laboratories, Naval Ocean Research and Development Activity (NORDA), Code 245, NSTL Station, MS 39529.

[1]H. S. W. Massey and D. R. Bates, Rep. Prog. Phys. **9**, 62 (1942).

[2]S. M. Razallah Ansari and Badre Alam, Sol. Phys. **41**, 97 (1975).

[3]Alan Burgess, Astrophys. J. **141**, 364 (1964).

[4]E. Källne, J. Källne, and J. I. Rice, Phys. Rev. Lett. **49**, 330 (1982).

[5]R. C. Elton and L. J. Palumbo, Phys. Rev. A **9**, 1873 (1974).

[6]Dennis L. Matthews, W. J. Braithwaite, Hermann H. Wolter, and C. Fred Moore, Phys. Rev. A **8**, 1397 (1973).

[7]Robert L. Kauffman, C. W. Woods, F. F. Hopkins, D. O. Elliott, K. A. Jamison, and Patrick Richard, J. Phys. B **6**, 2197 (1973).

[8]U. Feldman, G. A. Doschek, D. J. Nagel, W. E. Behring, and R. D. Cowan, Astrophys. J. **187**, 417 (1974).

[9]Chris A. Greene, Phys. Rev. A **23**, 661 (1974).

[10]P. G. Burke and P. D. McVicar, Proc. R. Soc. London **86**, 989 (1965).

[11]C. D. Lin, Phys. Rev. A **10**, 1986 (1984); Phys. Rev. Lett. **35**, 1150 (1975).

[12]C. P. Bhalla, A. H. Gabriel, and L. P. Presnyakov, Mon. Not. R. Astron. Soc. **172**, 359 (1974).

[13]J. A. Tanis, S. M. Shafroth, J. E. Willis, M. Clark, J. Swenson, E. N. Strait, and J. R. Mowat, Phys. Rev. Lett. **47**, 828 (1981).

[14]D. Brandt, Phys. Rev. A **27**, 1314 (1983).

[15]J. A. Tanis, E. M. Bernstein, W. G. Graham, M. Clark, S. M. Shafroth, B. M. Johnson, K. W. Jones, and M. Meron, Phys. Rev. Lett. **49**, 1325 (1982).

[16]Philip L. Pepmiller, Ph.D. dissertation, Kansas State University, 1983 (unpublished).

[17]Philip L. Pepmiller, Patrick Richard, J. Newcomb, R. Dillingham, J. M. Hall, Tom J. Gray, and M. Stockli, IEEE Trans. Nucl. Sci. **NS-30**, 1002 (1983).

[18]Philip L. Pepmiller and Patrick Richard, Phys. Rev. A **26**, 786 (1982).

[19]M. A. Blohkin, in *Methods of X-Ray Spectroscopic Research*, edited by M. A. S. Ross (Pergamon, New York, 1965), p. 176.

[20]A. J. Burek, D. M. Barrus, and R. L. Blake, Astrophys. J. **191**, 533 (1974).

[21]H. Tawara, Patrick Richard, K. A. Jamison, Tom J. Gray, J. Newcomb, and C. Schmiedekamp, Phys. Rev. A **19**, 1960 (1979).

[22]H. Tawara, Patrick Richard, K. A. Jamison, and Tom J. Gray, J. Phys. B **11**, L615 (1978).

[23]Patrick Richard, Philip L. Pepmiller, and K. Kawatsura, Phys. Rev. A **25**, 1937 (1982).

[24]M. D. Brown, L. D. Ellsworth, J. A. Guffey, T. Chiao, E. W. Pettus, L. W. Winters, and J. R. Macdonald, Phys. Rev. A **10**, 1255 (1974).

[25]M. J. Seaton and P. J. Storey, in *Atomic Processes and Applications,* edited by P. G. Burke and B. L. Moiseiwitsch (North-Holland, Amsterdam, 1976), Chap. 6.

[26]D. J. McLaughlin and Yukap Hahn, Phys. Lett. A **88**, 394 (1982).

[27]Larry J. Roszman, in *Physics of Electronic and Atomic Collisions,* edited by S. Datz (North-Holland, Amsterdam, 1982), p. 641.

[28]F. Biggs, L. B. Medelsohn, and J. B. Mann, At. Data Nucl. Data Tables **16**, 201 (1975).

[29]Detlev Brandt (private communication).

[30]C. P. Bhalla and T. W. Tunnell (private communication).

[31]C. Can and C. P. Bhalla, Proceedings of the 1982 Conference on the Application of Accelerators in Research and Industry [IEEE Trans. Nucl. Sci. **NS-30**, 1090 (1983)].

[32]K. LaGattuta and Y. Hahn (private communication).

[33]J. H. McGuire and C. L. Cocke (unpublished); D. Belkic and A. Salin, J. Phys. B **9**, L397 (1976).

[34]M. R. C. McDowell and J. P. Coleman, in *Introduction to the Theory of Ion-Atom Collisions* (North-Holland, Amsterdam, 1970), Chap. 4; D. R. Bates, in *Atomic and Molecular Processes,* edited by D. R. Bates (Academic, New York, 1962), p. 549.

[35]J. H. McGuire and P. L. Pepmiller (unpublished). The calculations are based on Ref. 34.

[36]K. Kawatsura, P. Richard, P. L. Pepmiller, J. M. Hall, T. R. Dillingham, and J. Newcomb, Phys. Rev. A (to be published).

[37]M. Clark, Bull. Am. Phys. Soc. **28**, 802 (1983).